ECS Transactions, 57 (1) 2573-2582 (2013)
10.1149/05701.2573ecst ©The Electrochemical Society

Electrode Reoxidation in Solid-Oxide Cells: Detailed Modeling of Nickel Oxide Film Growth

Jonathan P. Neidhardt[a,b], Robert J. Kee[c] and Wolfgang G. Bessler[d]

[a] German Aerospace Center, Institute of Technical Thermodynamics, Stuttgart, Germany
[b] Institute of Thermodynamics and Thermal Engineering, Stuttgart University, Germany
[c] Mechanical Engineering, Colorado School of Mines, Golden, Colorado, USA
[d] Offenburg University of Applied Sciences, Offenburg, Germany

The lifetime and performance of solid-oxide fuel cells (SOFC) and electrolyzer cells (SOEC) can be significantly degraded by oxidation of nickel within the electrode and support structures. This paper documents a detailed computational model describing nickel oxide (NiO) formation as a growing film layer on top of the nickel phase in Ni/YSZ composite electrodes. The model assumes that the oxidation rate is controlled by transport of ions across the film (Wagner's theory). The computational model, which is implemented in a two-dimensional continuum framework, facilitates the investigation of alternative chemical reaction and transport mechanisms. Model predictions agree well with a literature experimental measurement of oxidation-layer growth. In addition to providing insight in interpreting experimental observations, the model provides a quantitative predictive capability for improving electrode design and controlling operating conditions.

Introduction

Multiple mechanisms of performance degradation limit the lifetime of solid-oxide fuel cells (SOFC) and electrolyzer cells (SOEC). One well-known mechanism is the oxidation of nickel (Ni) within the electrode and support structures. The formation of nickel oxide (NiO) can cause significant performance losses due to triple phase boundary (TPB) reduction and blocking of free pore space (1). Furthermore, the volume expansion due to higher molar volume of NiO compared to Ni causes mechanical stresses inside the porous anode structure (2), which can cause anode extension (3,4), cracks (5,6) and delamination from the electrolyte (7).

Oxidation of the nickel phase can take place via two different pathways, that is, thermochemical and electrochemical oxidation (8). The thermochemical oxidation reaction takes place at the interface between metallic nickel and gas phase and is driven by molecular oxygen (O_2) or a high water content of the fuel gas (9,10),

$$Ni + \tfrac{1}{2} O_2 \rightleftarrows NiO \quad [1]$$

$$Ni + H_2O \rightleftarrows NiO + H_2 \quad [2]$$

In contrast, the electrochemical oxidation reaction occurs at the interface between nickel and the electrolyte phase (11,12),

$$Ni + O^{2-}[YSZ] \rightleftarrows NiO + 2\,e^{-}[Ni] \qquad [3]$$

Here the metal is oxidized by oxygen ions from the electrolyte, releasing electrons. This mechanism takes place, for example, upon operation at low cell voltages or an interruption of the fuel supply during galvanostatic SOFC operation.

In our previous work (13), both mechanisms have been implemented in a 2D continuum model of a solid oxide cell. The model allows calculating concentration and potential gradients inside the electrodes, as well as the resulting formation and dissolution of a bulk nickel oxide phase. Furthermore the prediction of local and global conditions for 'safe' and 'unsafe' cell operation is possible.

Aim of the present study is to obtain a more fundamental understanding on oxidation kinetics as well as on microstructural effects of NiO formation. For this purpose we describe the growth of nickel oxide as a thin film at the interface between nickel and the adjacent phase (gas phase or YSZ). The model assumes that the oxidation rate is controlled by transport of ions and vacancies across the film.

Fundamental work has been published by Wagner in 1933 (14), who described the growth of a metal oxide by transport of ions inside the thickening film. A detailed review is provided by Atkinson (15). More recently, Yu et al. described the transport inside NiO by first-principle calculations (16). Models describing the transport of charged species through solid phases in electrochemical systems have been developed by Kee and co-workers (17,18). It is agreed that the (thermochemical) growth of NiO over a wide range of temperatures is governed by vacancy diffusion of doubly-charged nickel ions (Ni^{2+}). It is accompanied by diffusion of electrons for maintenance of local charge neutrality (15). Additionally, the diffusion of oxygen interstitials (O^{2-}) can take place. Measurements by Chevalier et al. show that for temperatures > 1073 K the O^{2-} and Ni^{2+} diffusion coefficients have a similar magnitude (19).

Modeling and Simulation Methodology

Computational domain

Figure 1 illustrates the basic layout of the computational domain. Nickel oxide is modeled as flat film in one Cartesian dimension *z*. The film has two interfaces, where chemical and/or electrochemical reactions with the adjacent phases (e.g., bulk Ni, gas phase or YSZ) take place. Inside the film species transport is described via diffusion and migration.

Using a multi-scale approach, the film model is integrated into a 1D+1D continuum model of a single solid oxide cell (*x* and *y* dimensions) (20,21). Specifically, individual 1D film domains are included into every grid point of the macroscopic model, giving rise to an overall 1D+1D+1D multi-scale model. For the results presented here, only one grid point is used on the macro-scale.

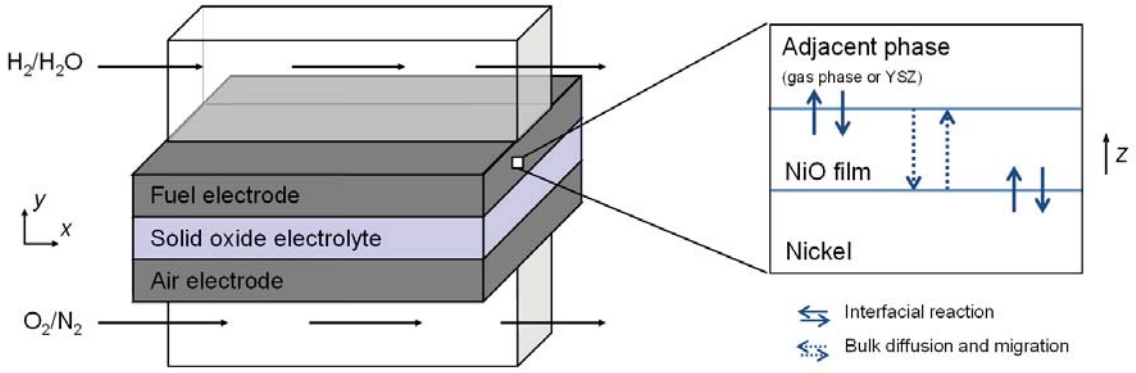

Figure 1. Illustration of the modeling domain for description of NiO growth, consisting of a 1D+1D model of an SOC and a coupled 1D model of the nickel oxide film. The *x* dimension is along the gas channels, the *y* dimension through the MEA thickness, and the *z* dimension through the nickel oxide film.

Film model

Growth of the film phase is controlled by transport of charged species inside the film. We apply the Nernst-Planck equation for evaluation of the species concentrations over time,

$$\frac{\partial c_i}{\partial t} = \nabla \cdot \left(D_i \nabla c_i + \frac{z_i c_i D_i F}{RT} \nabla \phi \right) \quad , \qquad [4]$$

with concentration c_i, diffusion coefficient D_i and charge number z_i of species *i*. ϕ, F, R and T denote electrical potential, Faraday's constant, ideal gas constant and temperature, respectively. Local electrical charge neutrality (EN) is assumed and introduced as additional governing equation,

$$\sum z_i c_i = 0 \quad . \qquad [5]$$

Boundary conditions for the transport equation are given by the species fluxes J through the interfaces, which can be expressed in terms of chemical rates,

$$J_i\big|_{\text{interface}} = \dot{s}_{i,\text{interface}} \quad , \qquad [6]$$

where $\dot{s}_{i,\text{interphase}}$ (in $\text{mol}\cdot\text{m}^{-2}\cdot\text{s}^{-1}$) is the heterogeneous molar production rate of species *i* at the interface.

The changes in volume fraction of the film phase and the adjacent phases are quantified by a multi-phase modeling approach, which was described earlier (21). We solve for the volume fractions $\varepsilon(t, x, y)$ of all phases inside the cell as a function of time and spatial location, by taking into account the chemical rate laws of all involved reactions and mass conservation (continuum approach). As a consequence, the thickness of the film δ can be described as function of its volume fraction,

$$\delta = \frac{\varepsilon_{\text{film}}}{A^{\text{V}}} \quad , \qquad [7]$$

where A^{V} is the volumetric surface area of the film interfaces. Both interfaces are assumed to have the same area.

SOC model

The film model is coupled into a two-dimensional continuum model of a solid oxide cell (20,21). For the present simulations, we use only one single grid point in the electrodes, that is, we ignore transport of gaseous species in channels and porous electrodes. This allows focusing on the effect of a given gas-phase composition or an applied potential on growth of the nickel oxide film, while still allowing for realistic boundary conditions.

Air electrode electrochemistry is described using a modified Butler-Volmer equation introduced by Zhu and co-workers (22). Current-voltage relationships are modeled by solving for the electric-potential distribution in the electrodes and electrolyte. The cell voltage E is defined as difference between cathode and anode potential step (20),

$$E = \phi_{\text{ca}} - \phi_{\text{an}} \quad . \qquad [8]$$

Parameterization

For reliable prediction of nickel oxide film growth the model has to be parameterized properly. For all species inside the film, thermodynamic properties (molar enthalpies and entropies) and diffusion coefficients are required, as well as the kinetic coefficients (preexponential factors, activation energies, symmetry factors) of (electro-)chemical reactions between NiO and the adjacent phases (nickel, gas-phase and YSZ). A summary of all film model parameters is given in Table 1. While thermodynamic data and diffusion coefficients are known from literature, the interfacial reactions can only be assumed. Reaction kinetics are chosen such, that species transport through the film is the rate-limiting step for NiO formation for $X_{\text{O}_2} = 1$ (10) during thermochemical oxidation, and for $E = 0.1$ V during electrochemical oxidation. For low oxygen partial pressures or high cell voltages the oxygen incorporating step can become rate determining (Eq. 12 or Eq. 15). The initial film NiO thickness is set to 10^{-10} m.

Numerical implementation

The model is written in C/C++ code and implemented into the in-house software package DENIS (detailed electrochemistry and numerical impedance simulation) (20,21). The film is treated as special case of a bulk phase, where the equations for bulk transport are solved (Eqs. 4–5). Chemical source terms are evaluated using CANTERA (23), which is coupled to DENIS on the code level. The computational domain is spatially discretized using the finite-volume method. For modeling a film with variable thickness the size of the discretization grid is adapted in each calculation step. Details are given in the Appendix. The resulting system of differential-algebraic (DAE) and ordinary differential equations (ODE) is solved using LIMEX (24).

TABLE I. Model parameters for NiO film growth (T = 1073 K).

Film species	**Thermodynamic data (h, s)**	**Ref.**	**Diffusion data (D_0, E_a)**	**Ref.**
Ni^{2+}	80 kJ mol^{-1}, 0 J mol^{-1} K^{-1}	(25)	4.3×10^{-5} m^2 s^{-1}, 171.7 kJ mol^{-1}	(26)
O^{2-}	-182 kJ mol^{-1}, 17.7 J mol^{-1} K^{-1}	(27)	17.7×10^{-2} m^2 s^{-1}, 259.8 kJ mol^{-1}	(19)
e^-	0, 0		4.3×10^{-5} m^2 s^{-1}, 171.7 kJ mol^{-1}	(26)
Interface NiO/Ni (thermo- and electrochemical oxidation)			**Kinetic data (k^f)**	**Eq.**
$Ni \rightleftarrows Ni^{2+}$[film] + 2 e^-[film]			1×10^2 m $kmol^{-1}$ s^{-1}	[9]
Ni^{2+}[film] + O^{2-}[film] $\rightleftarrows$ NiO			1×10^{-3} m^4 $kmol^{-1}$ s^{-1}	[10]
e^-[film] $\rightleftarrows$ e^-[Ni]			1×10^{-6} m $kmol^{-1}$ s^{-1}	[11]
Interface NiO/Gas (thermochemical oxidation)			**Kinetic data (k^f)**	**Eq.**
O_2 + 4 e^-[film] $\rightleftarrows$ 2 O^{2-}[film]			5×10^{-3} m^4 $kmol^{-1}$ s^{-1}	[12]
Ni^{2+}[film] + O^{2-}[film] $\rightleftarrows$ NiO			1×10^{-1} m^4 $kmol^{-1}$ s^{-1}	[13]
2 H_2O $\rightleftarrows$ 2 H_2 + O_2			1×10^5 m $kmol^{-1}$ s^{-1}	[14]
Interface NiO/YSZ (electrochemical oxidation)			**Kinetic data (k^f)**	**Eq.**
O^{2-}[film] + V[YSZ] $\rightleftarrows$ O^{2-}[YSZ]			6×10^{-8} m^4 $kmol^{-1}$ s^{-1}	[15]
Ni^{2+}[film] + O^{2-}[film] $\rightleftarrows$ NiO			1×10^{-1} m^4 $kmol^{-1}$ s^{-1}	[16]

Results and Discussion

Thermochemical oxidation

For simulating thermochemical oxidation we assume that the reduced nickel electrode is exposed to oxygen at different mole fractions (X_{O_2} = 1, 0.1, 10^{-2}, 10^{-3}, 10^{-4}, 10^{-5}) in binary O_2/N_2 mixtures, and alternatively to pure water vapor. The counterelectrode is exposed to air. Total pressure of 1.013 bar and temperature of 1073 K are assumed. We consider a growing NiO film with interfaces to the gas phase (NiO/gas) and to bulk Ni (NiO/Ni), with the respective reactions given in Table 1. The electrode is assumed to consist of a solid nickel block with a thickness of 100 µm. This assumption offers the possibility of direct comparison to experiments by Atkinson (26); realistic geometries occurring in SOFC electrodes will be investigated below.

Figure 2a shows simulated NiO film growth for this case. Solid lines indicate the film thickness as function of time for X_{O_2} = 1, the simulation shows good agreement with experimental data by Atkinson (26). This profile shows a parabolic shape, which is well-known to correspond to a growth process where bulk diffusion is the rate-limiting step (28). Decreasing oxygen pressures cause a decreased oxidation rate and simultaneously an increasing deviation from parabolic behavior. The deviation is caused by different kinetics during the beginning of the oxidation process. For a small film thickness and low oxygen pressure the rate-limiting process changes from bulk transport to surface reaction (28). Most probably the oxygen reduction reaction is the rate-limiting step under these conditions. This effect is very prominent for oxidation in water vapor (X_{H_2O} = 1). In this case, the simulated profile shows completely linear oxidation kinetics in the depicted time span.

This interpretation is supported by the concentration profiles shown in Figure 2b. For X_{O_2} = 1 (solid lines) the concentrations of nickel ions and electrons show a strong gradient. Concentrations are about zero at the NiO/gas interface and increase throughout the film. Due to imposed local charge neutrality, electron concentration is twice the Ni^{2+} concentration, while oxygen ion concentration is low. The electrical potential shows only a small gradient. These results are in agreement with the profiles for diffusion-limited film growth predicted by Atkinson (15). However, for $X_{O_2} = 10^{-5}$ (dotted lines) a different behavior can be observed. Here, concentrations of all species are nearly constant. This shows that the rate-limiting step for Ni oxidation has changed from diffusion to the oxygen reduction reaction (Eq. 12) for low oxygen partial pressures.

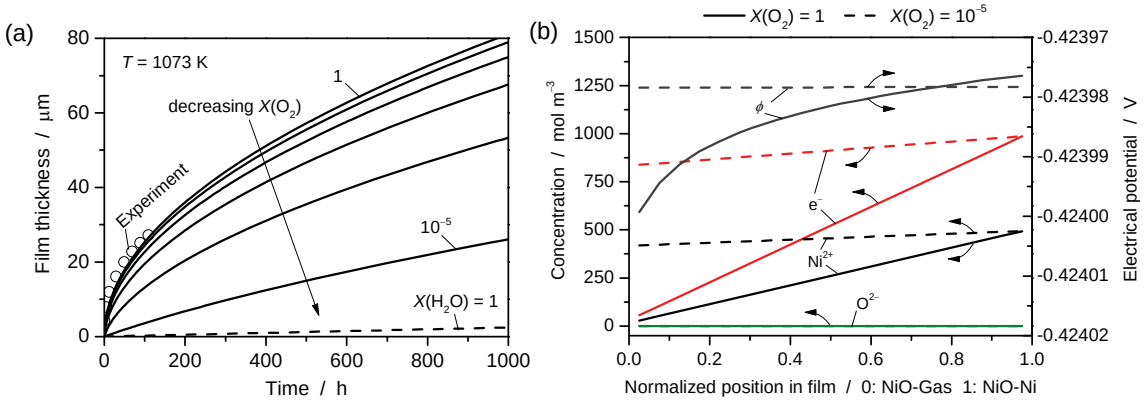

Figure 2. (a) Simulated NiO film growth via thermochemical Ni oxidation in comparison to measurements by Atkinson et al. (26) (b) Species concentration profiles and electrical potential distribution inside the film at 100 h for X_{O_2} = 1 and $X_{O_2} = 10^{-5}$.

Electrochemical oxidation

For simulating electrochemical oxidation, we assume that the nickel electrode is exposed to nitrogen to avoid any reactions of nickel with the gas phase. We assume a growing NiO film with interfaces to Ni (NiO/Ni) and YSZ (NiO/YSZ), with the respective reactions given in Table 1. The counterelectrode is exposed to air. Figure 3a shows simulated NiO film growth for different cell voltages *E* (solid lines). Comparison to thermochemical oxidation by X_{O_2} = 1 (dotted line) shows that electrochemical oxidation is faster than thermochemical oxidation for voltages < 0.4 V. Oxidation kinetics do not show parabolic behavior. For *E* = 0.4 V the deviation is clearly visible by comparison to the profile for X_{O_2} = 1. For low film thickness oxidation kinetics are slower than parabolic, but for high thickness they are faster. Lower voltages show the same behavior. For high cell voltages (*E* > 0.4 V) profiles are quasi-linear indicating a surface reaction as rate-limiting step (28).

Concentration profiles for all species and the electrical potential are shown for two voltages (*E* = 0.1 V and *E* = 0.6 V) in Figure 3b. Species profiles are very similar to the case of thermochemical oxidation (cf. Figure 2b). For *E* = 0.1 V transport of nickel ions is rate-limiting, while for *E* = 0.6 V the oxidation is controlled by oxygen transfer into the NiO (Eq. 16). However, in contrast to thermochemical oxidation, a large potential gradient of about 0.4 V can be observed for *E* = 0.1 V. This gives a possible explanation

for the fast kinetics for electrochemical oxidation shown in Figure 2a. Due to the potential gradient an additional migration flux can support the transport of nickel ions, allowing for faster film growth.

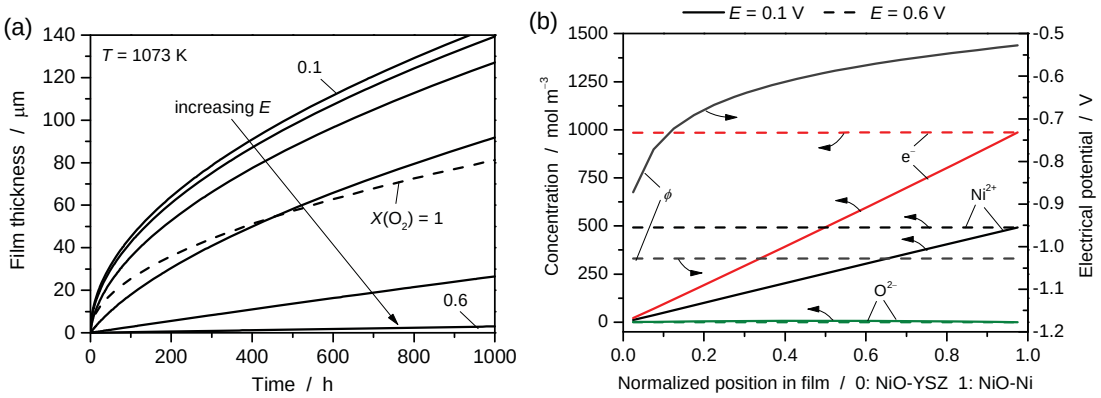

Figure 3. (a) Simulated NiO film growth via electrochemical Ni oxidation. The dashed line shows results for thermochemical oxidation (Fig. 2). (b) Species concentration profiles and electrical potential distribution inside the film after 100 h for cell voltages of E = 0.1 V and E = 0.6 V.

Combined model

Combination of thermochemical and electrochemical oxidation is simulated by assuming a 1 µm thick nickel layer with two individual NiO films, yielding a "stack" YSZ/NiO/Ni/NiO/Gas, where the left-hand side allows electrochemical oxidation while the right-hand side allows thermochemical oxidation. This allows the simulation of competition of both processes. Furthermore the conditions that occur locally during SOC operation (13) can be reproduced.

Figure 4 shows oxidation of the nickel layer upon thermochemically and electrochemically strongly oxidative conditions (X_{O_2} =1, E =0.1 V). The counterelectrode is exposed to air. In a time span of 3.8 min the complete nickel (solid line) is oxidized to a growing film of NiO from the interface to the gas phase (dotted line) as well as a second film forming at the interface to YSZ (dashed line). Due to the increase of molar volume (10) the final nickel oxide layer has a total thickness of 1.52 µm, out of which 39 % were formed by the thermochemical and 61 % by the electrochemical process.

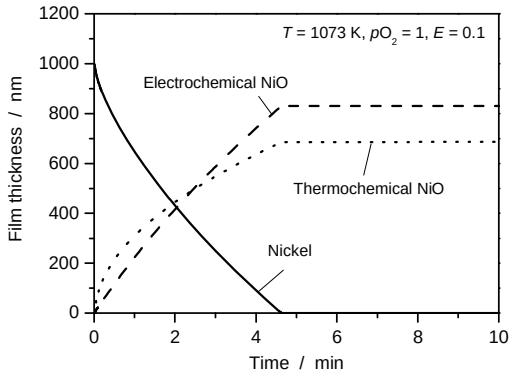

Figure 4. Competition of thermochemical and electrochemical film growth during oxidation of a nickel layer with 1 µm thickness.

Summary and Conclusions

We have modeled the growth of nickel oxide in solid oxide cells. NiO is described as a flat one-dimensional film. The model can successfully reproduce oxidation by molecular oxygen or water from the gas phase (thermochemical oxidation) as well as oxidation by oxygen ions from the YSZ electrolyte, driven by a potential gradient (electrochemical oxidation). In case of thermochemical oxidation, good agreement to a measurement by Atkinson et al. (26) is obtained. Simulations show that for high oxygen partial pressures ($X_{O_2} > 10^{-5}$) and for low cell voltages ($E < 0.4$ V) transport of nickel ions in the film is the rate-limiting step for film layer growth. At lower oxygen pressures or higher cell voltages our model predicts a growth which co-limited by oxygen incorporation into the NiO at the interfaces. Electrochemical oxidation is a potentially faster process than thermochemical oxidation because the occurring potential gradient supports species transport via migration.

Coupling of both oxidation mechanisms in a combined model can give insight into properties at real SOC operation conditions. Simultaneous oxidation from two interfaces increases the speed of oxidation. At the presented conditions (T = 1073 K, X_{O_2} = 1, E = 0.1 V) a nickel layer of 1 μm thickness is completely oxidized in a time span of 3.8 min.

The presented model is the basis for further investigations on nickel oxide formation under SOC operating conditions, aiming at a more fundamental understanding of electrode degradation mechanisms. Future simulations can provide a quantitative predictive capability for improving electrode design and controlling operating conditions.

Acknowledgments

Financial support for this work was provided by the Initiative and Networking Fund of the Helmholtz Association.

Appendix: Derivation of adaptive grid size adjustment

Modeling of a film with variable thickness requires the introduction of a discretization mesh with adaptive grid sizes. By defining grid sizes as fraction of the film thickness, the absolute compartment size can be recalculated in each calculation step,

$$dz_j = \zeta_j \delta \quad , \qquad [17]$$

where dz is the absolute size and ζ the fraction of grid compartment j with respect to the film thickness δ.

To achieve mass conservation of the species inside the film upon changing grid sizes the species conservation equation (Eq. 4) has to be extended by an additional source term. This is illustrated in Figure 5: If grid sizes are changed relative to film thickness (Eq. 7) a growing film results in an apparent increase of average concentration. Concentration c of a species inside the film can be written as,

$$c_i = \frac{n_i}{\delta \cdot A^{\mathrm{V}}} \quad , \qquad [18]$$

where n_i is the absolute amount of species i. Under the condition of a constant n_i and assuming a fixed surface area, derivation with respect to time gives the required corrective source term,

$$\frac{\partial c_i}{\partial t} = -\frac{n_i}{\delta^2 A^{\mathrm{V}}} \cdot \frac{\partial \delta}{\partial t} = -\frac{c_i}{\delta} \cdot \frac{\partial \delta}{\partial t} \quad . \qquad [19]$$

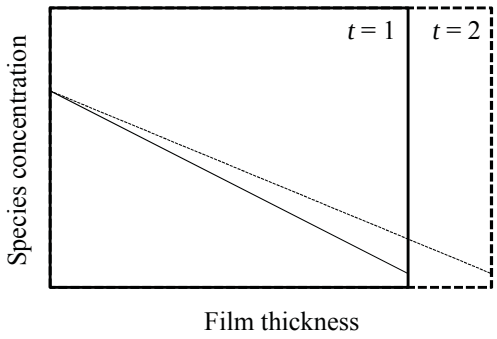

Figure 5. Illustration of concentration overestimation due to adaptive grid size adjustment. This is fixed by a correction term which is added to the species conservation equation.

References

1. T. Matsui, R. Kishida, J.-Y. Kim, H. Muroyama and K. Eguchi, *J. Electrochem. Soc.*, **157** (5), B776 (2010).
2. T. Klemenso, C. Chung, P.H. Larsen and M. Mogensen, *J. Electrochem. Soc.*, **152** (11), A2186 (2005).
3. A. Faes, A. Hessler-Wyser, D. Presvytes, C.G. Vayenas and J. Van Herle, *Fuel Cells*, **9** (6), 841 (2009).
4. M. Pihlatie, A. Kaiser and M. Mogensen, *Solid State Ionics*, **180** (17), 1100 (2009).
5. M. Ettler, H. Timmermann and J. Malzbender, A. Weber, N.H. Menzler, *J. Power Sources*, **195** (17), 5452 (2010).
6. D. Sarantaridis, R.A. Rudkin and A. Atkinson, *J. Power Sources*, **180** (2), 704 (2008).
7. J. Laurencin, G. Delette, B. Morel, F. Lefebvre-Joud and M. Dupeux, *J. Power Sources*, **192** (2), 344 (2009).
8. J. Neidhardt, M. Henke and W.G. Bessler, *ECS Trans.*, **35** (1), 1621 (2011).
9. G. Stathis, D. Simwonis, F. Tietz, A. Moropoulou and A. Naoumides, *J. Mater. Res.*, **17** (5), 951 (2002).
10. D. Sarantaridis and A. Atkinson, *Fuel Cells*, **7** (3), 246 (2007).
11. C.-H. Wang, M.-C. Lee, T.-J. Huang, Y.-C. Chang, W.-X. Kao and T.-N. Lin, *Electrochem. Commun.*, **11** (7), 1381 (2009).
12. T. Hatae, Y. Matsuzaki and Y. Yamazaki, *Solid State Ionics*, **179** (7-8), 274 (2008).
13. J.P. Neidhardt and W.G. Bessler, *J. Power Sources*, submitted (2013).
14. C. Wagner, *Z. Phys. Chem. B*, **21** (25) (1933).
15. A. Atkinson, *Rev. Mod. Phys.*, **57** (2), 437 (1985).
16. J. Yu, K.M. Rosso and S.M. Bruemmer, *J. Phys. Chem. C*, **116** (2), 1948 (2012).
17. A.M. Colclasure, K. a. Smith and R.J. Kee, *Electrochim. Acta*, **58**, 33 (2011).
18. R.J. Kee, H. Zhu, B.W. Hildenbrand, E. Vollestad, M.D. Sanders and R.P. O'Hayre, *J. Electrochem. Soc.*, **160** (3), F290 (2013).
19. S. Chevalier, F. Desserrey and J.P. Larpin, *Oxid. Met.*, **64** (3-4), 219 (2005).
20. W.G. Bessler, S. Gewies and M. Vogler, *Electrochim. Acta*, **53** (4), 1782 (2007).
21. J.P. Neidhardt, D.N. Fronczek, T. Jahnke, T. Danner, B. Horstmann and W.G. Bessler, *J. Electrochem. Soc.*, **159** (9), A1528 (2012).
22. H. Zhu, R.J. Kee, V.M. Janardhanan, O. Deutschmann and D.G. Goodwin, *J. Electrochem. Soc.*, **152**, A2427 (2005).
23. D.G. Goodwin, Cantera: An Object-oriented Software Toolkit for Chemical Kinetics, Thermodynamics, and Transport Processes, Caltech, Pasadena (2009).
24. P. Deuflhard, E. Hairer and J. Zugck, *Num. Math.*, **51** (5), 501 (1987).
25. P. Kofstad, *Oxid. Met.*, **44** (1-2), 3 (1995).
26. A. Atkinson, R. Taylor and A. Hughes, *Philos. Mag. A*, **45** (5), 823 (1982).
27. J. Park and C. Altstetter, *Mater. Trans. A*, **18A** (1), 43 (1987).
28. P. Kofstad, High-Temperature Oxidation of Metals, John Wiley & Sons, New York (1966).